Peer Reviewed Paper openaccess

Hyperspectral imaging of the degradation of meat and comparison with necrotic tissue in human wounds

Amadeus Holmer,[a,*] Christoph Hornberger,[b] Thomas Wild[c] and Frank Siemers[d]

[a]Diaspective Vision GmbH, Strandstraße 15, D-18233 Am Salzhaff, Germany

[b]Faculty of Engineering, University of Applied Sciences Wismar, Phillip-Müller-Str. 14, D-23952 Wismar, Germany

[c]Clinic of Dermatology, Immunology and Allergology, Medical Center Dessau, Auenweg 38, D-06847 Dessau-Roßlau, Germany

[d]BG-Kliniken Bergmannstrost, Postfach 200153, D-06002 Halle (Saale), Germany

The objective evaluation of scattering tissue and the discrimination of tissue types is an issue that cannot be solved with colour cameras and image processing alone in many cases. Examples can be found in the determination of freshness and ageing of meat, and the discrimination of tissue types in food technology. In medical applications tissue discrimination is also an issue, e.g. in wound diagnostics. A novel hyperspectral imaging setup with powerful signal analysis algorithms is presented which is capable of addressing these topics. The spectral approach allows the chemical analysis of material and tissues and the measurement of their temporal change. We present a method of hyperspectral imaging in the visible-near infrared range which allows both the separation and spatial allocation of different tissue types in a sample, as well as the temporal changes of the tissue as an effect of ageing. To prove the capability of the method, the ageing of meat (slices of pork) was measured and, as a medical example, the application of the hyperspectral imaging setup for the recording of wound tissue is presented. The method shows the ability to discriminate the different tissue components of pork meat, and the ageing of the meat is observable as changes in spectral features. An additional result of our study is the fact that some spectral features, which seem to be typical for the ageing of the meat, are similar to those observed in the necrotic tissue from wound diagnostics in medicine.

Keywords: hyperspectral imaging, food monitoring, meat freshness, objective wound assessment, necrotic tissue, VIS-NIR spectroscopy

Introduction

Hyperspectral imaging (HSI) combines spectroscopy with imaging and therefore allows the analysis of the spatial distribution of the chemical composition of samples. In recent years HSI has found its way into several areas such as environmental science, agriculture, food, pharmaceuticals, medicine and others.[1] In the food industry it is used, amongst other applications, for monitoring meat quality and analysis of meat composition (muscle, intramuscular fat, subcutaneous fat, water etc.).[2–4]

Due to its non-invasiveness, HSI in the visible and near infrared (NIR) spectral range from 500 nm to 1000 nm has been proved to provide a large amount of relevant information about physiological parameters (e.g. blood volume, tissue oxygenation, water content) in different

Correspondence
Amadeus Holmer (amadeus.holmer@diaspective-vision.com)

Received: 4 December 2017
Revised: 27 February 2019
Accepted: 25 March 2019
Publication: 4 April 2019
doi: 10.1255/jsi.2019.a9
ISSN: 2040-4565

Citation
A. Holmer, C. Hornberger, T. Wild and F. Siemers, "Hyperspectral imaging of the degradation of meat and comparison with necrotic tissue in human wounds", *J. Spectral Imaging* **8,** a9 (2019).
https://doi.org/10.1255/jsi.2019.a9

medical application areas like diabetic foot and skin ulcers,[5–7] tissue perfusion measurements, wound analysis and flap monitoring.[8–10] Benefits of this methodology are the contact-free measurement without the need for contrast agents or other invasive procedures.

The field of wound treatment is a cost-intensive clinical field. In Germany, 2–4 billion euros are spent on the treatment of chronic wounds annually.[11] 1–2 million patients suffer from chronic wounds each year. Almost half of the costs arise from clinical care. Reasons for this are the limited possibilities for diagnosis and the lack of objectification of the affected areas. In the field of flap surgery, severe problems can occur if circulatory disorders are detected too late. This creates high costs due to the need for additional operations and extended hospitalisation times.

Tissue that is dead and has changed chemically is termed necrotic, however, at present there is no terminology for tissue which will become necrotic without treatment. One reason for this may be that there is no applicable or cost-effective and, therefore, comprehensive way of assessing wounds objectively.

Although the investigation of meat quality and wound diagnostic have nothing in common at first glance, light–tissue interaction is comparable. The irradiated light is scattered and absorbed by substantial structures and components of the skin and other specific tissue components, the spectrally modified remitted light transports information about the structure of the tissue (structure analysis) and the states of components (chemical analysis). Porcine models are widely used in NIR spectroscopy medical research. Although it is known that porcine hemoglobin differs from human haemoglobin, resulting in different absorption coefficients (see Reference 12 and references therein) many authors use the porcine model for tissue optical investigations.[13,14]

From suggestion of light path simulations,[15,16] the remission spectroscopic measurement in the visible range (500–650 nm) provides information about the superficial parts of the tissue, and the measurement in the NIR range (650–1000 nm) provides information about deeper layers of the tissue. Deeper layer in this context means deeper than 1 mm. From known optical properties of human skin,[17] typical light penetration depth can be estimated to be between approximately 0.8 mm (500 nm) and 2.6 mm (1000 nm).

Additional to information on the deeper part of the tissue, information on chemical components like water and fat content can be accessed. One of the major benefits of HSI is that the spectroscopic measurements are not just point measurements as in NIR spectroscopy techniques, but are performed over an area, so that spatial structures of the measured area can be evaluated in connection with the local spectral information using, for instance, segmentation procedures.

In this study, slices of pork (slices of the lower leg) were analysed with HSI over a period of seven days in the spectral range 500–1000 nm. We studied the change of spectral features of different regions (connective tissue, bone, muscle, fat and skin) and tried to compare specific spectral features with those features observable in medical applications of HSI, especially with necrotic areas from wound diagnostic research.

Materials and methods

Instrumental settings

HSI, or chemical imaging, is the combination of spectroscopy, imaging data acquisition and digital image processing. The setup for the meat observations is shown in Figure 1. The hyperspectral camera (TIVITA® Tissue, Diaspective Vision GmbH, Germany) was mounted on a desk stand with a flexible extension arm. The distance to the meat was set to 50 cm. The camera was connected to an industrial PC system that was equipped with 128 GB

Figure 1. TIVITA™ Tissue hyperspectral camera mounted on a flexible extension arm and plate with the meat.

SSD and 1 TB HDD, 16 GB DDR4 RAM and an Intel Core i3 dual-core processor (3.7 GHz).

The design of the new compact HSI camera includes an internal push broom imaging spectrograph used for spectral data acquisition along the x-axis (acquiring a full spectrum for every point of the row in parallel), a high-quality, infrared enhanced CMOS megapixel camera sensor (CMOSIS CMV 2000 3E12), integrated in an intelligent camera with USB3 data transfer for high recording speed and an internal stepper motor moving the slit of the spectrograph (and the spectrograph itself) at the first image plane of the optical setup along the y-axis to realise the image acquisition.

The imaging spectrograph is optimised for compact and lightweight construction which enables the camera to be used for precise and fast scanning. A transmission configuration with an optimised high efficiency holographic grating (>50 % efficiency) is used for high light efficiency. The internal spectrometer unit (including the sensor) is calibrated for wavelength and the system is smile corrected.

For the measurement shown in the results, a varifocal lens with a fixed focal length of 12 mm and an aperture of f1.4 was used. A long-pass optical filter (Schott, GG 495) with additional anti-reflection coating with a cut-off below 495 nm was mounted in front of the objective lens to suppress the second order of light intensities below 495 nm.

The resolution of the data cube is scalable by software and was set to 640 × 480 spatial points with a spectral resolution of 100 spectral bands between 500 nm and 1000 nm. The recorded data are calculated and converted from radiance to reflectance (according to Equation 1) in the software and the resulting values are stored as single precision float (32-bit). The data-size of the cubes are therefore 122 Mbyte.

The illumination of the entire investigation area of 21 × 28 cm is provided by an illumination unit containing six halogen lamps with a total power consumption of 120 W. The six single spots are arranged during production so that the resulting area is illuminated nearly uniformly without the need for additional diffusion elements.

To observe the meat over a longer period of time and also at night, the halogen lighting unit could be activated by software. Increased temperature due to light emission can accelerate meat degradation. To measure this effect, the temperature of the room and the meat was taken before each measurement and the illumination was deactivated after each measurement to limit the influence as much as possible.

As the temperature of the sensor increases as a result of prolonged use or due to long exposure times, the dark current effects (black level) and the noise of the sensor increases drastically. Because the sensor has no built-in black level correction method, compensation has to be performed separately. The CMOS sensor noise pattern was recorded during the setup of the camera. It includes fixed pattern noise and hot pixels that are not corrected by the intelligent camera itself. The black level of the sensor is recorded from non-illuminated sensor areas and corrected after recording the data cube by the system software.

To convert image data from radiance to diffuse reflectance, a white reference cube was taken by recording a cube from a white reference object before the measurements started. This also balances regional differences of the lighting. The previously recorded dark pattern is taken into account during the white balancing. For the white reference object, a sheet of uncoated white paper was used, characterised by a high diffuse reflectance with linear spectral distribution over the measured wavelength range from 500 nm to 1000 nm.

The camera parameterisation and data acquisition were performed by LabView-based software (TIVITA® Suite, Diaspective Vision GmbH, Germany). This software controls the data acquisition process (including balancing and wavelength calculating steps) and automatically performs data analysis to determine perfusion-related parameters from the HSI data cube for medical applications.

For the long-term observation of the meat over seven days, the software was modified in order to enable the automatic activation of the lighting unit. Also, all user dialog boxes and the preview image were deactivated so it was not necessary for an operator to observe the measurements all the time. Furthermore, the images were stored directly in a built-in database. A total of 74 measurements were recorded for meat observation.

The camera including the optical setup that was used for the clinical measurements of the necrosis and hematoma was exactly the same as the meat measurement setup, but the serial numbers of the cameras and the camera-dependent calibration parameters were different. For the clinical measurements, the camera was mounted on a flexible medical cart unit instead of the table mounting unit that was used for the meat measurements. The PC

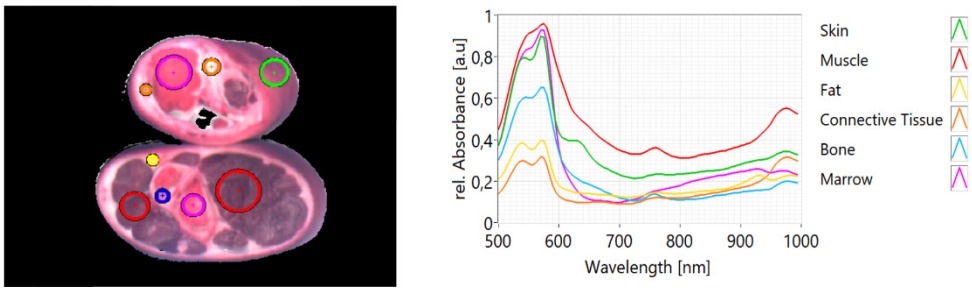

Figure 2. Hyperspectral image of the meat five hours after taking the meat out of the cooler with a) RGB colour image representation with marker positions and b) absorbance spectra of the marker positions of a).

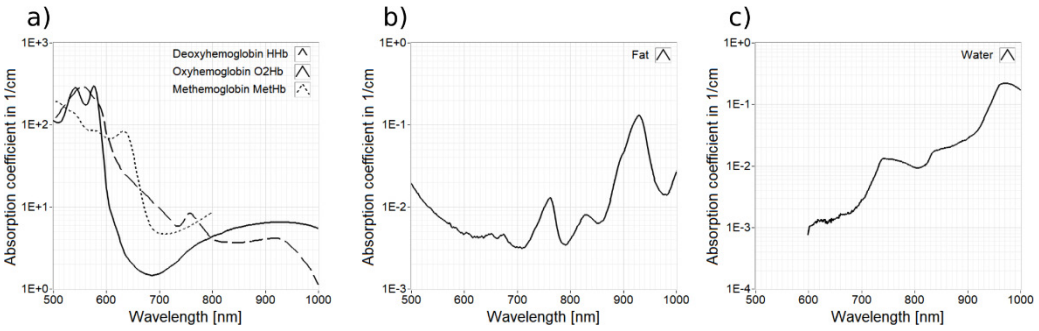

Figure 3. Molar extinction coefficients of a) oxyhemoglobin O_2Hb, deoxyhemoglobin HHb[18] and methemoglobin MetHb,[19] b) fat[20] and c) water.[21]

system, software including the calculations and spectral calibrations, and the peripheral equipment was similar in both parts of the study. The clinical necrosis and hematoma measurements were recorded only once and should be thought of as case studies.

Data acquisition and analysis

For the measurements, slices of the lower leg of a pig were used. The pig was slaughtered and dissected two days before start of the measurements. Before the measurements started, the meat was stored at a temperature of 2–6 °C, which resulted in a high degree of freshness. After the meat had been removed from the refrigerator, it was placed on a plate under the hyperspectral camera and measured at a room temperature of 19 °C for the rest of the experiment.

Figure 2 a) shows the hyperspectral image as an RGB colour representation with different tissue types marked and Figure 2 b) shows the corresponding mean absorbance spectra of each type. The absorbance A is calculated from the diffuse reflectance R with Equation 1.

$$A = -\log_{10} R = -\log_{10}\left(\frac{I}{I_0}\right) \quad (1)$$

Here I_0 is the incoming intensity and I the reflected intensity. The different tissues are distinguishable by their characteristic spectral features. In the range from 500 nm to 600 nm, hemoglobin and myoglobin are the main absorbers. The literature extinction spectra of pure deoxygenated (HHb) and oxygenated hemoglobin (O_2Hb),[18] methemoglobin (MetHb),[19] fat[20] and water[21] are given in Figure 3 for the purpose of comparison. In tissue spectra, the typical structures of these spectra can be found, even if the exact shape deviates due to scattering influences and the influence of other absorbers. For example, the characteristic double-peak structure of the oxygenated hemoglobin is clearly visible in the spectra of connective tissue, fat, marrow and of skin. In the spectrum of muscle tissue and of bone, the significant absorption band at 760 nm caused by the deoxygenated hemoglobin is distinct. As expected, the absorption band of pure fat at 930 nm can be detected in the spectrum of the fat position, whereas the water absorbance at 960 nm is not recognisable. The same structure can be observed in the spectrum of marrow. The water peak is present significantly in the spectra of muscle and connective

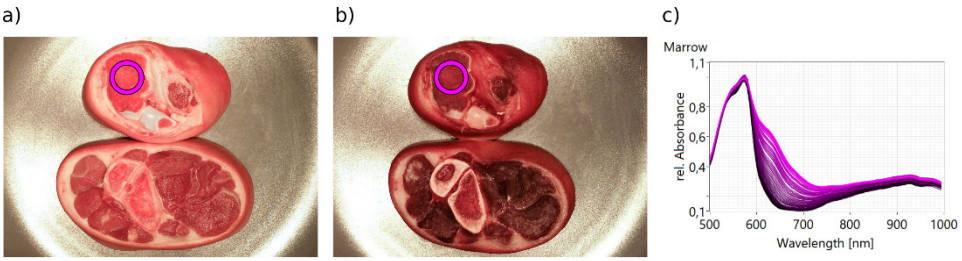

Figure 4. Colour photography of the meat a) after the meat warms to ambient temperature (3 h after taking the meat out of the cooler) and b) after the whole measurement period (7 d); c) absorbance spectra of marrow from all measurements. The later the measurement was taken, the more the colour saturation of the curves are increased. A constant increase of the absorbance of all wavelength could be observed. Between 600 nm and 750 nm, the absorbance increases more and continuously over the observation period. In the range from 500 nm to 580 nm, the increase of the absorbance is stronger in the first hours and remains stable after 8 h. The violet marker shows the area from which the spectra were taken.

tissue. Bone and skin show only a slight absorbance at this typical water band.

The spectrum of skin shows a significant unknown structure between 600 nm and 650 nm, which is not visible in other spectra.

The observations give a subtle hint that these spectral features may allow the different tissue types to be discriminated. Further studies and the application of classification models are needed to test this hypothesis. In addition, a change of the tissue characteristics during ageing of the meat is observable in the recorded hyperspectral imaging data in the visible and NIR range. An example of this is shown for marrow tissue: a colour photo of the fresh meat [Figure 4 a)] and the meat at the end of the measuring period of seven days [Figure 4 b)] is presented, and the absorbance spectra of one specific area inside the bone marrow (indicated with a violet marker) are given in Figure 4 c). The spectra of all pixels inside the marker area were taken and averaged to get one mean spectrum. Figure 4 c) shows the mean spectra for all (72) taken measurements. In one mean spectrum 1162 single spectra are included.

In the photo at the end of the measurement period, Figure 4 b), nearly every tissue type has darkened with the exception of the outer edge of the bone where the colour becomes brighter and the contrast to the marrow has increased. Also, the shape of the meat has changed. The skin, especially, has become firm and shrunken.

In Figure 4 c) the marrow spectra over the whole observation period is displayed, the colouring of the spectra has intensified over time. Here the darkening of the meat is observable in the absorbance spectra as an increase of absorbance over time. As the meat loses water over time, the concentration of absorbers (e.g. the hemoglobin components oxygenated and deoxygenated hemoglobin) is increased resulting in a higher absorbance. In the range from 500 nm to 600 nm, the increase of absorbance is stronger in the first hours and remains nearly stable after eight hours. Between 600 nm and 750 nm, the absorbance increases more and continuously over the observation period. Especially at 630 nm, a new absorption band is formed which we cannot assign directly to one of the known chromophores. The first spectra (black curves) show a double-peak structure between 500 nm and 600 nm. This structure is typical of oxygenated hemoglobin. There is no significant peak visible at 760 nm, indicating that the present hemoglobin is not significantly deoxygenated. Also, the water absorption peak at 960 nm cannot be observed, but a peak structure at 930 nm is present that is characteristic of fat that is part of bone marrow.

In Figure 5, the absorbance changes over time for all tissue types are plotted as the mean spectrum of the whole amount of different number of pixels. The spectra were recorded every 24 hours, the colour saturation of the plotted spectra increases with time. Because the sizes of the different tissue type structures are different, the size of the markers and, therefore, the number of the used pixels are also different. The number of pixels for each spectrum are: bone 278, connective tissue 270, skin 1162, fat 178, marrow 1162 and muscle 2843. In the absorbance spectrum of connective tissue, Figure 5 e),

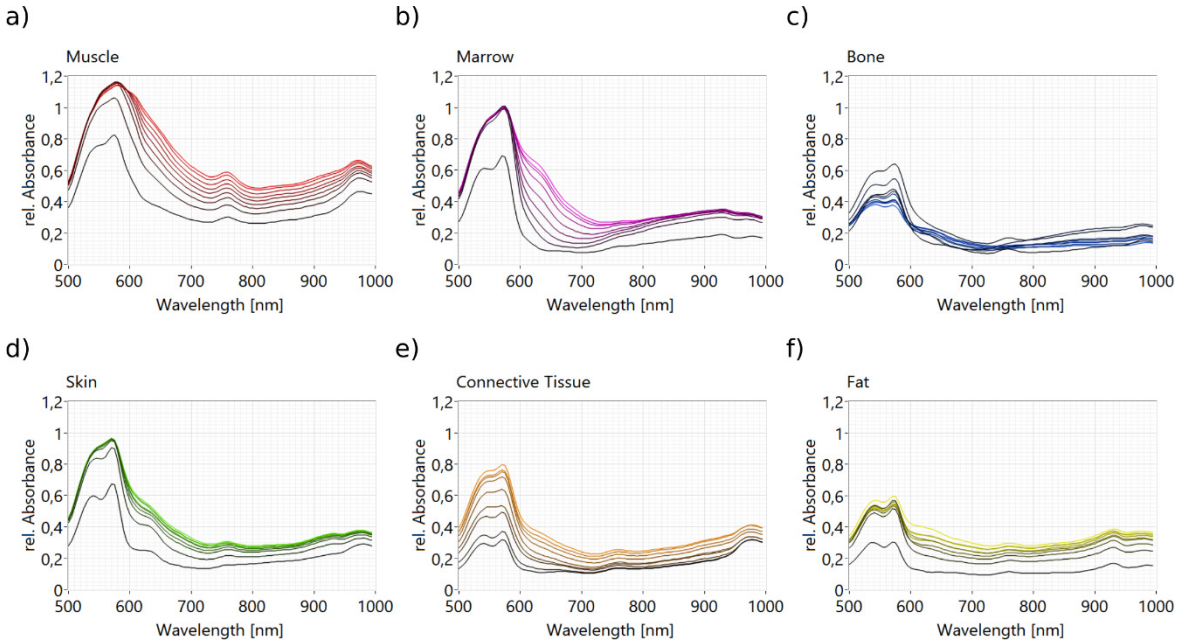

Figure 5. Absorbance spectrum of all marker positions from Figure 2 from a selection of measurements with a) muscle tissue, b) marrow, c) bone, d) skin, e) connective tissue and f) fat. The later the measurement was taken, the more the colour saturation of the curves are increased. The measurements were taken with a time difference of 24 h.

where a prominent water peak at 960 nm is present, the absorption in the range 500–600 nm becomes dominant over the 960 nm water peak over time. This may be due to the dewatering of the connective tissue over time. In muscle tissue, this effect is not visible at first glance. It can be easily seen that the changes over time are different in different wavelength regions and the changes proceed with varying rates. As the changes beside dewatering are caused by chemical reactions such as oxygenation and deoxygenation, the hyperspectral imaging method allows the reactions and the reactions rates to be observed. Although we cannot provide a full analysis of the chemical processes involved, we can assume a change of the oxygenation status of hemoglobin being responsible for most changes in the double-peak structure between 500 nm and 600 nm (O_2Hb) and in the peak at 760 nm (HHb).

In Figure 6, standard normal variate (SNV)-transformed absorbance spectra over time of muscle tissue (a), marrow (b), bone (c), skin (d), connective tissue (e) and fat (f) are shown with

$$x_{i,SNV} = \frac{\left(x_i - \overline{x}\right)}{\sqrt{\frac{\sum_{i=1}^{P}\left(x_i - \overline{x}\right)^2}{p-1}}} \qquad (2)$$

where $\overline{x}$ is the mean value over all absorptions of all wavelength and the denominator is the standard deviation over all spectra values.

With SNV, the mean value is set to zero and the standard deviation is scaled to a value of one, so that offsets are removed from the spectra and spectral shifts or relative changes in the absorption band intensities become clearly visible. The SNV transformation was also used in Reference 22 as a pre-treatment of pork spectra. The spectral characteristics of pre-processed spectra of meat have been used by different authors to discriminate between tissue types or different pre-treated meat or different states of freshness. In References 23 and 24, the wavelength range 400–1050 nm was used to discriminate between frozen and unfrozen prawns and pork, respectively. We also use the spectral characteristics to discriminate tissue types and the change of the tissue due to ageing. In Figure 6 a) it can be seen that there are relative changes in the water absorption band at 960 nm and in the range from 600 nm to 700 nm. The shape of the deoxygenation band at 760 nm is nearly the same for the whole observation period, indicating that there is no significant change of the oxygenation. This shows that the spectral change between 600 nm and 700 nm is not caused by a change of oxygenation.

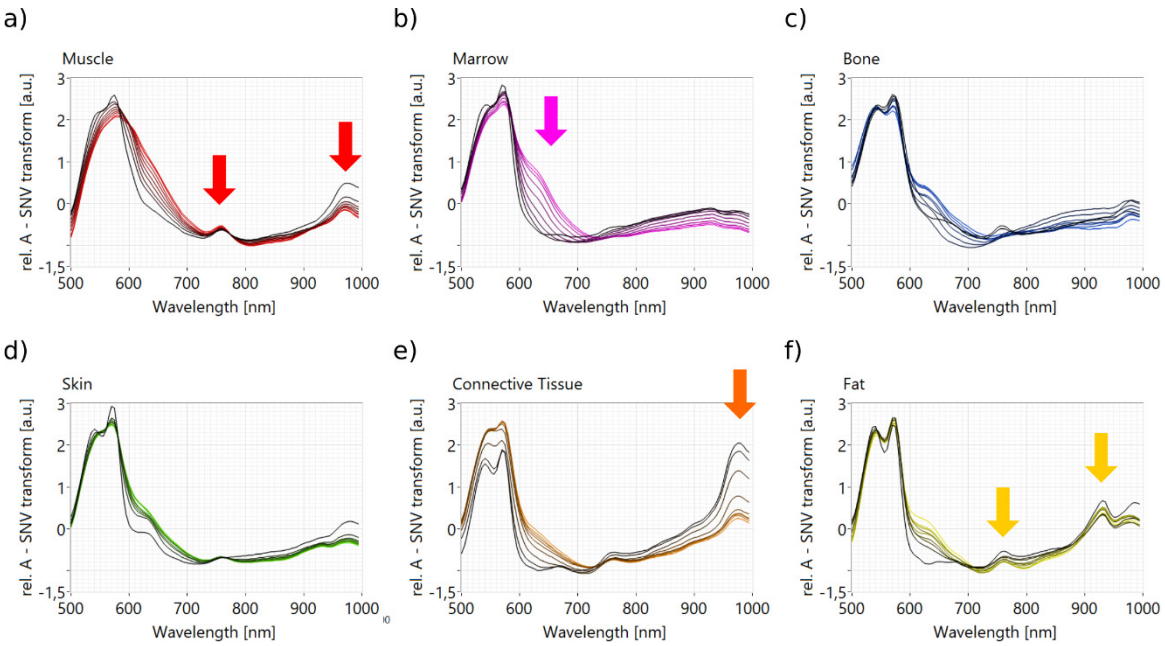

Figure 6. SNV-transformed absorbance spectrum of a) muscle tissue, b) marrow, c) bone, d) skin, e) connective tissue and f) fat. There are different spectral features for each substance clearly visible (marked with arrows).

The relative decrease of the spectral band at 960 nm shows that the water content decreases and the meat dries. In the fat spectra, Figure 6 f), the typical fat peak at 930 nm is clearly visible. In addition, a peak at 760 nm occurs. Because the double-peak structure in the range from 500 nm to 600 nm indicates a high oxygenation of the hemoglobin part of the spectrum, this structure at 760 nm cannot be the spectrum of deoxygenated hemoglobin and must be an influence of the fat spectrum that shows a significant structure in this region [compare with Figure 3 b)]. The decrease of water could also be observed for the spectra of connective tissue, Figure 6 e). The structure in the range from 720 nm to 770 nm has a different shape from that in the spectra of muscle tissue. It is possible that this is also an influence of the water absorbance in this region and not the peak of deoxygenated hemoglobin. In the spectra of marrow, Figure 6 b), the emergence of the specific shoulder between 600 nm and 700 nm is clearly visible.

Results and discussion

Hyperspectral imaging is suitable for classifying different tissue types in meat by specific spectral features. The ageing or rather deterioration of meat is observable as changes in spectral features and there is potential to deduce the rates of different ageing processes. The shoulder between 600 nm and 700 nm in Figure 5, which occurs most strongly in the absorbance spectra of marrow, is not yet understood but it is apparent that there must be some chemical changes of the tissue. Most likely, parts of the hemoglobin changes to new derivatives such as Methemoglobin MetHb or Sulfhemoglobin SHb as References 25 and 26 suggest.

In Figure 7 the hyperspectral image of a necrotic wound is displayed and for some specific wound regions the absorbance spectra are presented. In Figure 8 the hyperspectral image of a hematoma with the derived absorbance spectra is shown. Figure 9 shows a comparison of the different spectra from meat marrow and the clinical recorded images in one plot, after SNV transformation (a) and in relative absorbance (b). The absorbance spectra of necrotic tissue type 2 and of the hematoma reveal a shoulder between 600 nm and 700 nm as in the marrow spectra of the aged meat in Figure 5 b). This could be a hint that this specific spectroscopic feature between 600 nm and 700 nm, which is revealed during the ageing process, is caused by a process of tissue degradation to necrotic tissue. As mentioned above, the absorption coefficients of porcine hemoglobin and human hemoglobin differ and, therefore, a comparison of the spectra

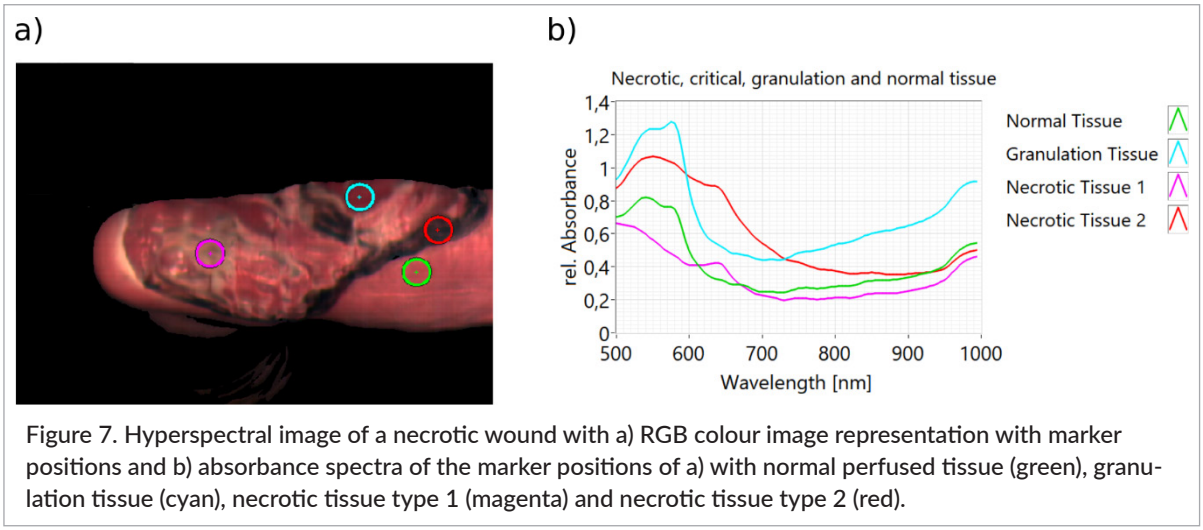

Figure 7. Hyperspectral image of a necrotic wound with a) RGB colour image representation with marker positions and b) absorbance spectra of the marker positions of a) with normal perfused tissue (green), granulation tissue (cyan), necrotic tissue type 1 (magenta) and necrotic tissue type 2 (red).

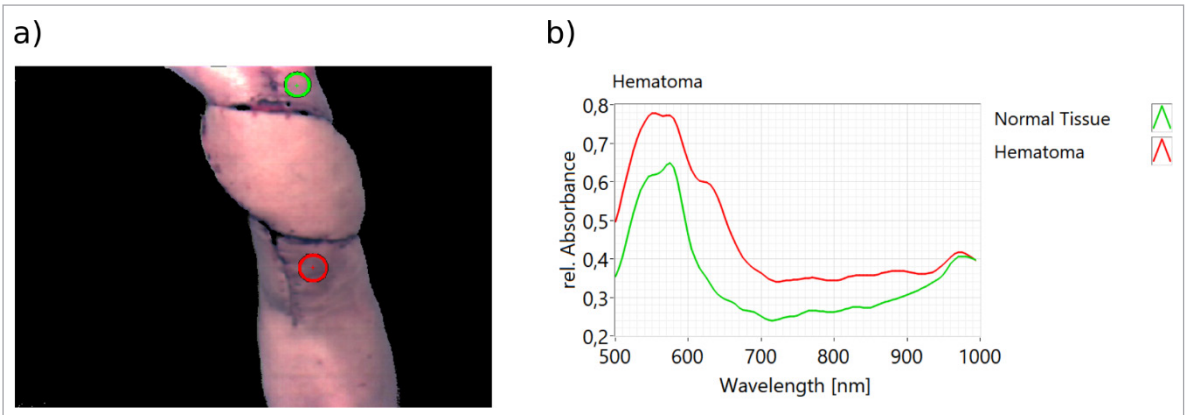

Figure 8. Hyperspectral image of a hematoma with a) RGB colour image representation with marker positions and b) absorbance spectra of the marker positions of a) with normal perfused tissue (green) and hematoma (red).

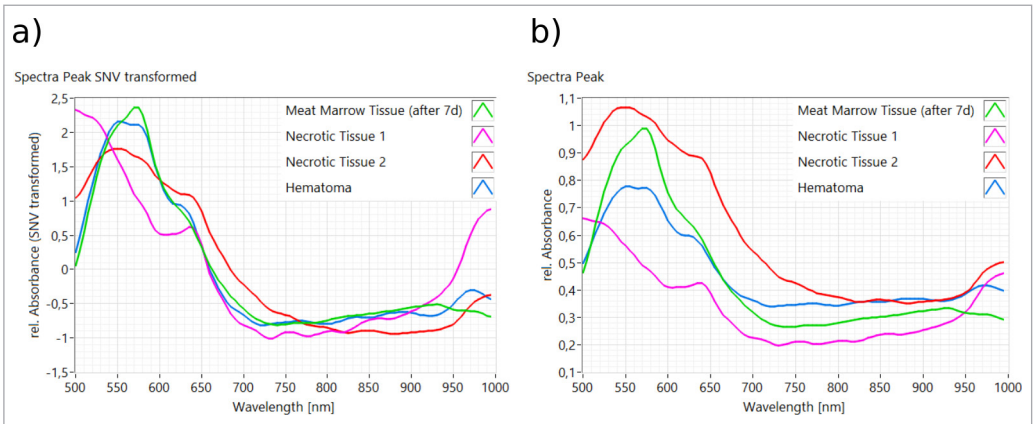

Figure 9. SNV-transformed (a) and relative absorbance spectra (b) of marrow after 7 d (green curve), necrotic tissue 1 (pink curve), necrotic tissue 2 (red curve) and hematoma (blue curve).

of aged meat and necrotic tissue is no evidence that the same or similar tissue components or hemoglobin derivates are present. On the other hand, the shape of the spectra of fresh meat are similar to those of a mixture of oxygenated and deoxygenated hemoglobin which can be measured in human applications. Therefore, the similarity of the shoulder in aged meat and necrotic tissue can be a hint that similar processes take place.

Not all of the spectral features of aged meat and wounds are fully understood, but it is apparent that hyperspectral imaging provides the tools to understand and analyse ageing processes of meat and is capable of supporting wound diagnosis. Further studies are needed to investigate whether the observed shoulder above 600 nm is caused by tissue degradation or hemoglobin derivatives which are generated during tissue degeneration.

Conclusion

The introduced hyperspectral imaging setup is suitable for tissue optical applications. The combination of hyperspectral imaging with powerful signal analysis algorithms enables the user to analyse specific spectral features, which is a prerequisite for any discrimination of image areas, e.g. segmentation of different tissue types. The presented examples of meat ageing and necrotic wound tissue give rise to the assumption that similar decomposition processes are present.

References

1. A. Kumar, S. Saxena, S. Shrivastava, V. Bharti, U. Kumar and K. Dhama, "Hyperspectral imaging (HSI): Applications in animal and dairy sector", *J. Exp. Biol. Agric. Sci.* **4(4),** 448–461 (2016). https://doi.org/10.18006/2016.4(4).448.461
2. G. Elmasry, D.F. Barbin, D.-W. Sun and P. Allen, "Meat quality evaluation by hyperspectral imaging technique: An overview", *Crit. Rev. Food Sci. Nutr.* **52(8),** (2012). https://doi.org/10.1080/10408398.2010.507908
3. J.M. Balage, S. da Luz E Silva, C.A. Gomide, M. de Nadai Bonin and A.C. Figueira, "Predicting pork quality using Vis/NIR spectroscopy", *Meat Sci.* **108,** 37–43 (2015). https://doi.org/10.1016/j.meatsci.2015.04.018
4. M. Kamruzzaman, Y. Makino and S. Oshita, "Online monitoring of red meat color using hyperspectral imaging", *Meat Sci.* **116,** 110–117 (2016). https://doi.org/10.1016/j.meatsci.2016.02.004
5. D. Yudovsky, A. Nouvong and L. Pilon, "Hyperspectral imaging in diabetic foot wound care", *J. Diabetes Sci. Technol.* **4(5),** 1099–1113 (2010). https://doi.org/10.1177/193229681000400508
6. M.S. Chin, B.B. Freniere, Y.-C. Lo, J.H. Saleeby, S.P. Baker, H.M. Strom, R.A. Ignotz, J.F. Lalikos and T.J. Fitzgerald, "Hyperspectral imaging for early detection of oxygenation and perfusion changes in irradiated skin", *J. Biomed. Optics* **17(2),** 026010 (2012). https://doi.org/10.1117/1.JBO.17.2.026010
7. A. Nouvong, B. Hoogwerf, E. Mohler, B. Davis, A. Tajaddini and E. Medenilla, "Evaluation of diabetic foot ulcer healing with hyperspectral imaging of oxyhemoglobin and deoxyhemoglobin", *Diabetes Care* **32(11),** 2056–2061 (2009). https://doi.org/10.2337/dc08-2246
8. K.J. Zuzak, M.D. Schaeberle, E.N. Lewis and I.W. Levin, "Visible reflectance hyperspectral imaging: Characterization of a noninvasive, *in vivo* system for determining tissue perfusion", *Anal. Chem.* **74(9),** (2002). https://doi.org/10.1021/ac011275f
9. M.A. Calin, T. Coman, S.V. Parasca, N. Bercaru, R.S. Savastru and D. Manea, "Hyperspectral imaging-based wound analysis using mixture-tuned matched filtering classification method", *J. Biomed. Optics* **20(4),** 046004 (2015). https://doi.org/10.1117/1.JBO.20.4.046004
10. G. Lu and B. Fei, "Medical hyperspectral imaging: A review", *J. Biomed. Optics* **19(1),** 010901 (2014). https://doi.org/10.1117/1.JBO.19.1.010901
11. S. Purwins, K. Herberger, E.S. Debus, S.J. Rustenbach, P. Pelzer, E. Rabe, E. Schäfer, R. Stadler and M. Augustin, "Cost-of-illness of chronic leg ulcers in Germany", *Int. Wound J.* **7(2),** 97–102 (2010). https://doi.org/10.1111/j.1742-481X.2010.00660.x
12. R. Serianni, J. Barash, T. Bentley, P. Sharma, J.L. Fontana, D. Via, J. Duhm, R. Bunger and P.D. Mongan, "Porcine-specific hemoglobin saturation measurements", *J. Appl. Physiol.* **94(2),** 561–566 (2003). https://doi.org/10.1152/japplphysiol.00710.2002
13. M. Firbank, C.E. Elwell, C.E. Cooper and D.T. Delpy, "Experimental and theoretical comparison of NIR

spectroscopy measurements of cerebral hemoglobin changes", *J. Appl. Physiol.* **85(5),** 1915–1921 (1998). https://doi.org/10.1152/jappl.1998.85.5.1915

14. R. Nosrati, S. Lin, A. Ramadeen, D. Monjazebi, P. Dorian and V. Toronov, "Cerebral hemodynamics and metabolism during cardiac arrest and cardiopulmonary resuscitation using hyperspectral near infrared spectroscopy", *Circulation J.* **81(6),** 879–887 (2017). https://doi.org/10.1253/circj.CJ-16-1225

15. B.H. Herrmann and C. Hornberger, "Monte-Carlo simulation of light tissue interaction in medical hyperspectral imaging applications", *Curr. Direct. Biomed. Eng.* **4(1),** 275–278 (2018). https://doi.org/10.1515/cdbme-2018-0067

16. P.D. Mannheimer, "The light-tissue interaction of pulse oximetry", *Anesthes. Analg.* **105(6),** S10–S17 (2007). https://doi.org/10.1213/01.ane.0000269522.84942.54

17. A.N. Bashkatov, E.A. Genina, V.I. Kochubey and V.V. Tuchin, "Optical properties of human skin, subcutaneous and mucous tissues in the wavelength range from 400 to 2000 nm", *J. Phys. D* **38(15),** 2543 (2005). https://doi.org/10.1088/0022-3727/38/15/004

18. *Molar Extinction Coefficients of Oxy and Deoxyhemoglobin*, compiled by S. Prahl. http://omlc.ogi.edu/spectra/hemoglobin [accessed April 2017].

19. W.G. Zijlstra, A. Buursma, and O.W. van Assendelft, *Visible and Near Infrared Absorption Spectra of Human and Animal Haemoglobin: Determination and Application*. VSP International Science Publ, Utrecht (2000).

20. R.L.P. van Veen, H.J.C.M. Sterenborg, A. Pifferi, A. Torricelli, E. Chikoidze and R. Cubeddu, "Determination of visible near-IR absorption coefficients of mammalian fat using time- and spatially resolved diffuse reflectance and transmission spectroscopy", *J. Biomed. Optics* **10(5),** 054004 (2005). https://doi.org/10.1117/1.2085149

21. S.J. Matcher, M. Cope and D.T. Delpy, "Use of the water absorption spectrum to quantify tissue chromophore concentration changes in near-infrared spectroscopy", *Phys. Med. Biol.* **39(1),** 177 (1994). https://doi.org/10.1088/0031-9155/39/1/011

22. D.F. Barbin, G. Elmasry, D.-W. Sun and P. Allen, "Predicting quality and sensory attributes of pork using near-infrared hyperspectral imaging", *Anal. Chim. Acta* **719,** 30–42 (2012). https://doi.org/10.1016/j.aca.2012.01.004

23. Q. Dai, J.-H. Cheng, D.-W. Sun, H. Pu, X.-A. Zeng and Z. Xiong, "Potential of visible/near-infrared hyperspectral imaging for rapid detection of freshness in unfrozen and frozen prawns", *J. Food Eng.* **149,** 97–104 (2015). https://doi.org/10.1016/j.jfoodeng.2014.10.001

24. H. Pu, D.-W. Sun, J. Ma and J.-H. Cheng, "Classification of fresh and frozen-thawed pork muscles using visible and near infrared hyperspectral imaging and textural analysis", *Meat Sci.* **99,** 81–88 (2015). https://doi.org/10.1016/j.meatsci.2014.09.001

25. A. Marrone and J. Ballantyne, "Changes in dry state hemoglobin over time do not increase the potential for oxidative DNA damage in dried blood", *PLoS ONE* **4(4),** e5110 (2009). https://doi.org/10.1371/journal.pone.0005110

26. T.L. Mollan, S. Banerjee, G. Wu, C.J. Parker Siburt, A.-L. Tsai, J.S. Olson, M.J. Weiss, A.L. Crumbliss and A.I. Alayash, "α-Hemoglobin stabilizing protein (AHSP) markedly decreases the redox potential and reactivity of α-subunits of human HbA with hydrogen peroxide", *J. Biol. Chem.* **288(6),** 4288–4298 (2013). https://doi.org/10.1074/jbc.M112.412064